The Flexibility of Long Chain Substituents Influences Spin-Crossover in Isomorphous Lipid Bilayer Crystals†‡

Iurii Galadzhun,[a] Rafal Kulmaczewski,[a] Namrah Shahid,[a] Oscar Cespedes,[b] Mark J. Howard[a] and Malcolm A. Halcrow*[a]

$[Fe(bpp)_2][BF_4]_2$ (bpp = 2,6-di{pyrazol-1-yl}pyridine) derivatives with a bent geometry of hexadec-1-ynyl or hexadecyl substituents pyrazole are isomorphous, and high-spin at room temperature. However, only the latter compound undergoes an abrupt, stepwise spin-transition on cooling. This may reflect the different conformational flexibilities of their long chain substituents.

Spin-crossover (SCO) compounds are molecular switches, where a change of spin state at a metal ion perturbs the colour, (para)magnetism, conductivity, dielectric constant and/or the volume of a material.[1-3] Such transitions can be triggered by physical or chemical stimuli, making SCO centres of interest for device applications; in switchable nanostructures for molecular electronics; or as reporters for chemical or physical sensors.[4] While most of this research is done with solid materials, SCO molecules bearing long chain substituents can form switchable liquid crystals, gels and micellar assemblies.[5-7] Other such materials show mesophase transitions[8] or isotropic melting[9] coupled to spin-state changes. Lastly, SCO compounds decorated with long chains can form crystals exhibiting unusual switching cooperativity reflecting conformational changes in the alkyl substituents during the SCO process.[10-14] However, other compounds bearing long chain substituents show more typical solid state SCO, where the alkyl chains have little effect on the form of the transition.[14,15]

We have reported derivatives of the $[Fe(bpp)_2]^{2+}$ (bpp = 2,6-di{pyrazol-1-yl}pyridine) family of SCO materials,[16] bearing long chain alkyl substituents at their pyridyl *C*4 positions. That gives a linear distribution of alkyl groups on the complex molecule.[17] While the structural chemistry of the complexes depended on their alkyl chain length, their spin state properties were more consistent, with most showing the onset of gradual SCO above 350 K. Appending alkyl chains to other sites on the heterocyclic skeleton should give differently shaped amphiphile complexes based on the same $[Fe(bpp)_2]^{2+}$ core. With that in mind, we now report new bpp derivatives bearing alkyl chains at just one pyrazolyl ring (Scheme 1), which yield a bent geometry of alkyl substituents about an $[Fe(L^1_n)_2]^{2+}$ or $[Fe(L^2_n)_2]^{2+}$ centre. We have found examples from both series which are isomorphous, but have unexpectedly different spin state properties.

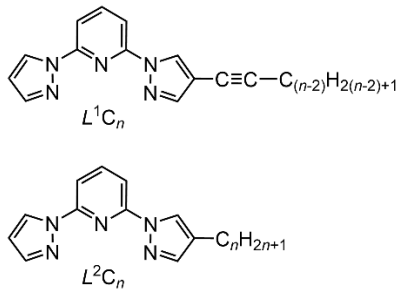

Scheme 1 The new ligands synthesised in the work (*n* = 12, 14, 16, 18).

Sonogashira coupling of 2-{iodopyrazol-1-yl}-6-{pyrazol-1-yl}pyridine with 1 equiv of the appropriate 1-alkyne afforded L^1C_n (*n* = 12, 14, 16 or 18) in yields of 34-48 %.[18] Hydrogenation of L^1C_n over Pd/C gave the corresponding alkylated derivatives L^2C_n in 54-94 % yield. X-ray crystal structures were obtained for L^1C_{12}, L^2C_{12} and L^2C_{14}. The alkynyl substituent in L^1C_{12} has a *gauche* torsion at the *C*3 position, which induces a *ca* 95° kink between its heterocyclic and alkyl domains. The molecules pack into bilayers in the lattice, with weak π-π overlap between their heterocyclic cores but no interdigitation of their alkyl groups. The alkyl chains in isomorphous L^2C_{12} and L^2C_{14} have no *gauche* torsions, and their alkyl and heterocyclic domains are almost coplanar. These molecules also associate into bilayers in the lattice, with alternating pairs of stacked heterocyclic cores and interdigitated alkyl chains (Figures S10-S13†).

[a]*School of Chemistry, University of Leeds, Woodhouse Lane, Leeds, UK LS2 9JT. E-mail: m.a.halcrow@leeds.ac.uk.*
[b]*School of Physics and Astronomy, University of Leeds, E. C. Stoner Building, Leeds LS2 9JT, UK*

‡ Data associated with this study are available from the University of Leeds library at http://doi.org/10.5518/974

† Electronic Supplementary Information (ESI) available: synthetic procedures and analytical data; crystallographic data and other experimental details; crystallographic Figures and Tables, and other characterisation data. CCDC 2064046-2064049. For ESI and crystallographic data in CIF or other electronic format see DOI: 10.1039/x0xx00000x

Iron tetrafluoroborate complexes of all these ligands were obtained in analytical purity, except $[Fe(L^1C_{18})_2][BF_4]_2$ which is not discussed further. While most complexes analysed as solvent-free materials, some contained 1-2 equiv lattice water by microanalysis and/or TGA. Single crystals were only obtained from the $[Fe(L^2C_n)_2][BF_4]_2$ series and, of these, only $[Fe(L^2C_{12})_2][BF_4]_2$ diffracted synchrotron radiation sufficiently well for a full structure refinement. Preliminary structure solutions from more weakly diffracting crystals of $[Fe(L^2C_{16})_2][BF_4]_2$ and $[Fe(L^2C_{18})_2][BF_4]_2$ confirmed these are isomorphous with the L^2C_{12} complex (Table S2†).

The asymmetric unit of $[Fe(L^2C_{12})_2][BF_4]_2$ contains two unique cation sites, which are both high-spin at 120 K (Figures 1 and S21, and Table S3†). Both ligands in each molecule have one *gauche* torsion, at the *C*2 position in one dodecyl chain and the *C*3 position of the other, which are oriented so the remainder of the chains are approximately co-parallel. The cations form bilayers in the (001) plane, with tightly packed interdigitated alkyl chains (Figure 1). The interlayer distance in the lattice is 29.592(3) Å, slightly less than the unit cell *c* dimension.[19] The $[Fe(bpp)_2]^{2+}$ core of each cation interacts with two nearest neighbours in the other half of its bilayer, through $\pi...\pi$ contacts between their unsubstituted pyrazolyl groups (Figure S22†). Interacting pairs of pyrazolyl rings are coplanar, and separated by 3.19(6) Å. The A and B cation environments are segregated within the bilayers by these interactions, into alternating π-stacked chains along the unit cell *a* axis (Figures S23-S25†).

Bulk samples of $[Fe(L^1C_{12})_2][BF_4]_2$ and $[Fe(L^1C_{14})_2][BF_4]_2$ are apparently isomorphous but poorly crystalline, and contain a significant amount of amorphous material by powder diffraction (Figure S28†). The compounds show similar magnetic behaviour in undergoing gradual, incomplete thermal SCO with midpoint temperatures ($T_{½}$) near 270 K (*n* = 12) and 290 K (*n* = 14; Figure S29†). Both materials exhibit constant $\chi_M T$ values of 1.2 $cm^3\ mol^{-1}\ K$ between 50-130 K, implying *ca* one-third of their iron sites remain high-spin at low temperature, with a typical zero-field splitting-induced decrease in $\chi_M T$ on cooling below 50 K.[20] We attribute this behaviour to the presence of both SCO-active and high-spin phases in the samples, corresponding to their crystalline or amorphous fractions. In contrast $[Fe(L^1C_{16})_2][BF_4]_2$ is more crystalline, adopts a different structure type, and shows no amorphous hump in its powder pattern (Figure 2). This compound is fully high-spin between 5-350 K (Figures 3 and S28†).

Room temperature powder diffraction of $[Fe(L^2C_n)_2][BF_4]_2$ (*n* = 12-18) implies they are isomorphous with each other, and with $[Fe(L^1C_{16})_2][BF_4]_2$; the powder patterns of $[Fe(L^1C_{16})_2][BF_4]_2$ and $[Fe(L^2C_{16})_2][BF_4]_2$ are almost identical (Figures 2 and S30†). That is supported by crystallographic unit cell data from compounds in the L^2C_n series (Table S2†). The (002), (003) and (004) reflections in each powder pattern are correlated and strongly enhanced while other reflections are weak or absent, especially for the shorter alkyl chain lengths. Since the cation bilayers lie in the (001) plane, that reflects the lamellar crystal packing in the materials.[21] The correlated (00*l*) 2θ values are significantly different in each material, and are consistent with the available crystallographic simulations (Figure S31†).

The powder pattern of $[Fe(L^2C_{12})_2][BF_4]_2$ resembles the other L^2C_n complexes, even though the bulk material contains 1-2 equiv lattice water by microanalysis, TGA and DSC whereas its single crystals are anhydrous. The flexibility of the dodecyl chains may allow water molecules to penetrate its lattice, without significantly changing its bilayer packing.[17]

Magnetic data from $[Fe(L^2C_n)_2][BF_4]_2$ show a consistent trend, of a thermal spin transition near 150 K which becomes more complete and better resolved as the chain length *n* increases. Thus $[Fe(L^2C_{12})_2][BF_4]_2{\cdot}H_2O$ remains almost entirely high-spin on cooling; $[Fe(L^2C_{14})_2][BF_4]_2{\cdot}H_2O$ shows a small SCO in *ca* 15 % of its iron centres; and $[Fe(L^2C_{16})_2][BF_4]_2$ and $[Fe(L^2C_{18})_2][BF_4]_2$ show more abrupt spin transitions proceeding to *ca* 60 % and 70 % completeness respectively (Figures 3 and S32†). In contrast to $[Fe(L^1C_n)_2][BF_4]_2$, the phase purity of these

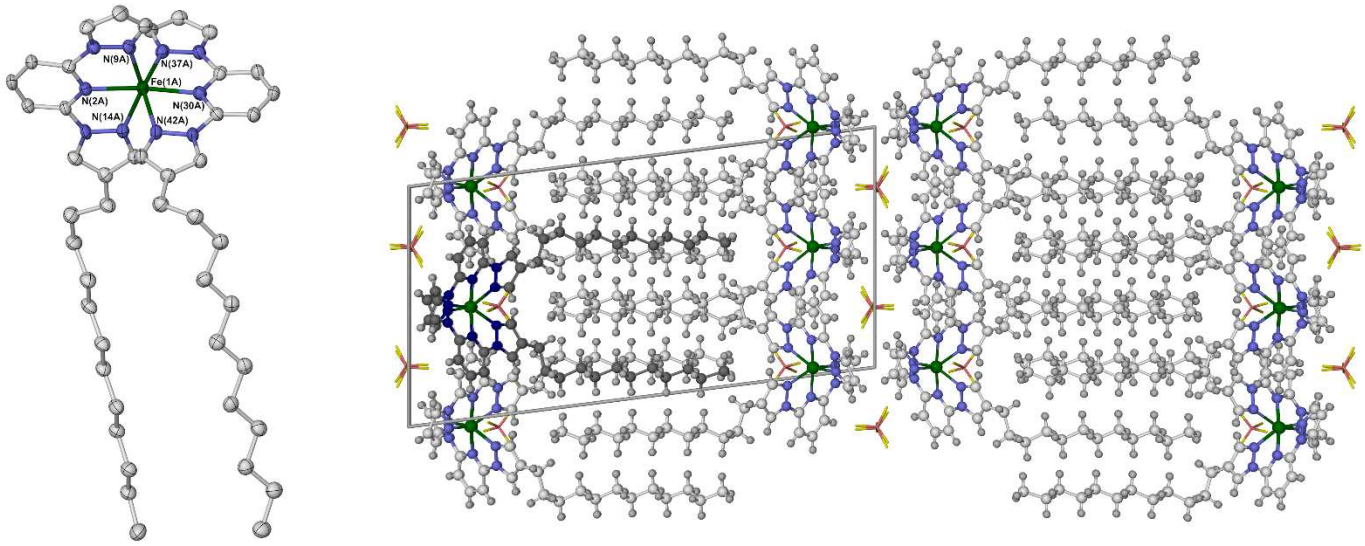

Figure 1 Left: one of the two unique complex cations in the asymmetric unit of $[Fe(L^2C_{12})_2][BF_4]_2$. Displacement ellipsoids are at the 50 % probability level, and H atoms are omitted for clarity. Right: packing diagram of $[Fe(L^2C_{12})_2][BF_4]_2$, viewed parallel to the [100] crystal vector, with *b* vertical. Atoms are plotted with arbitrary radii; one cation is highlighted with dark colouration; and the anions are de-emphasised, for clarity. Colour code: C, white or dark grey; H, pale grey; B, pink; F, yellow; Fe, green; N, pale or dark blue.

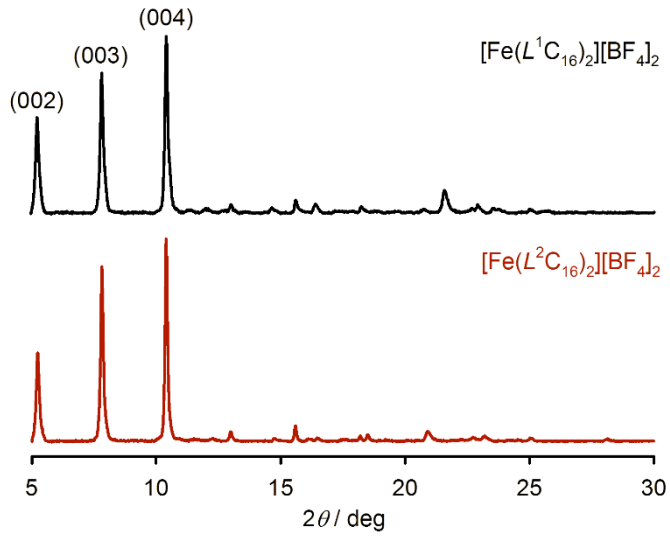

Figure 2 Room temperature X-ray powder diffraction patterns for $[Fe(L^1C_{16})_2][BF_4]_2$ (black) and $[Fe(L^2C_{16})_2][BF_4]_2$ (red). The assignment of the most intense peaks is shown, based on a simulated powder pattern from $[Fe(L^2C_{16})_2][BF_4]_2$ (Figure S30).

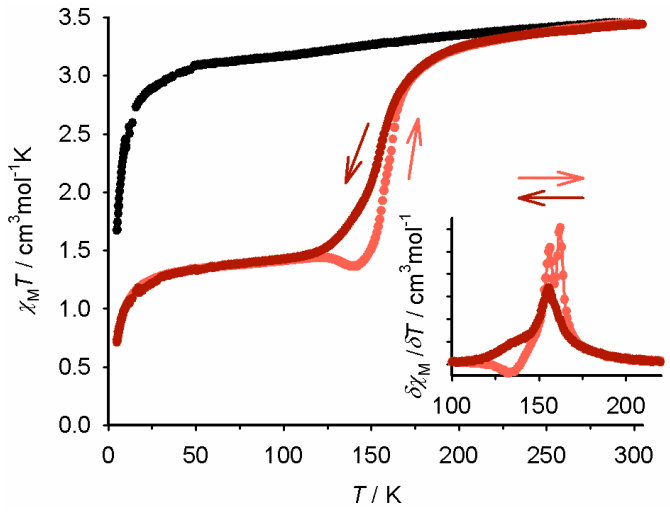

Figure 3 Magnetic susceptibility data for $[Fe(L^1C_{16})_2][BF_4]_2$ (black) and $[Fe(L^2C_{16})_2][BF_4]_2$ (red). The inset shows the first derivative of the data for $[Fe(L^2C_{16})_2][BF_4]_2$, whose cooling and warming scans have dark and pale colouration. Scan rate 5 K min^{-1}. The decrease in $\chi_M T$ below 50 K reflects zero-field splitting of the high-spin fraction of the samples.[20]

materials implies their incomplete SCO is more likely to reflect thermal trapping of the residual 30-40 % fraction of the samples in their high-spin state.[22-24] That is common in materials from the $[Fe(bpp)_2]^{2+}$ family whose SCO extends below *ca* 100 K.[23,24] This is supported by the small decrease in $\chi_M T$ near 130 K shown by $[Fe(L^2C_{16})_2][BF_4]_2$ in warming mode, indicating relaxation of the sample to its thermodynamic spin state population at that temperature (Figure 3). A repeat measurement of that compound at a faster scan rate of 10 K min^{-1} led to a less complete spin-transition and a more pronounced relaxation step on re-warming, confirming the kinetic origin of this behaviour (Figure S33†).[24,25]

The spin-transitions in $[Fe(L^2C_{16})_2][BF_4]_2$ and $[Fe(L^2C_{18})_2][BF_4]_2$ clearly proceed in two steps, with narrow thermal hysteresis (Figures 3 and S32†). For m = 16, the steps occur at $T_{½}$ = 149 K [$\Delta T_{½}$ = 15 K] and 159 K [6 K], and for m = 18 the parameters are $T_{½}$ = 150 K [$\Delta T_{½}$ = 15 K] and 166 K [2 K]. This hysteresis is likely to be kinetic in origin, based on the discussion in the previous paragraph.[26] The stepwise nature of the transitions is consistent with the two unique cation sites in the crystals of both compounds, which would be likely to undergo SCO independently of each other (Figures S26 and S27†).[27] Alternative explanations such as the involvement of a re-entrant intermediate crystal phase in the SCO process cannot be ruled out, however, since crystals of both compounds diffract too weakly for full structural characterisation.[28]

All the $[Fe(L^2C_n)_2][BF_4]_2$ compounds, and $[Fe(L^1C_{16})_2][BF_4]_2$, show a reversible endotherm by DSC at a temperature between 350-375 K (Figure S35†). This is not a mesophase transition, since the materials remain solid on heating to 443 K (Figure S36†). Hence, we tentatively assign it to a crystal-to-crystal phase transition.

The most striking aspect of this work is the different spin state properties of isomorphous $[Fe(L^1C_{16})_2][BF_4]_2$, which is high-spin, and SCO-active $[Fe(L^2C_{16})_2][BF_4]_2$ (Figure 3). That could be influenced by the conformational properties of an alkynyl *vs* an alkyl substituent, and by the electronic influence of those substituents on the metal ion ligand field.[29] To investigate the latter, magnetic measurements in solution were obtained for these compounds (Figure S37†). These showed $[Fe(L^1C_{16})_2][BF_4]_2$ undergoes SCO at $T_{½}$ = 247 ±2 K in CD_3CN, which is just 6 K below $[Fe(L^2C_{16})_2][BF_4]_2$ [$T_{½}$ = 252.8 ±0.5 K]. Hence, the inductive properties of the L^1C_{16} and L^2C_{16} ligand substituents are unlikely to be solely responsible for quenching SCO in $[Fe(L^1C_{16})_2][BF_4]_2$.

In conclusion, $[Fe(L^2C_n)_2][BF_4]_2$ exhibit a partial spin-transition near 150 K, which becomes more complete and better defined as n increases. When n = 16 and 18 the transition occurs abruptly and in two steps, which likely reflects the presence of two unique iron environments in their crystal lattice. In contrast $[Fe(L^1C_{16})_2][BF_4]_2$, which is isomorphous with the L^2_n complexes by powder diffraction, remains high-spin on cooling. This does not reflect the electronic character of the L^1R and L^2R ligands, but may instead be explained by the more rigid hexadec-1-ynyl substituents in the L^1C_{16} complex. The cooperative SCO shown by $[Fe(L^2C_{16})_2][BF_4]_2$ and $[Fe(L^2C_{18})_2][BF_4]_2$ is also unusual for materials bearing such long-chain alkyl spacers. However, it is noteworthy that other iron(II) complexes with a bent disposition of alkyl chains also exhibit cooperative and structured spin-transitions in the solid state.[12-14] A bent amphiphile geometry may be particularly suited to cooperative spin-transitions in lipid bilayer materials.

This work was funded by the the University of Leeds and the EPSRC (EP/K012568/1 and EP/N509681/1). We thank Diamond Light Source for access to beamline I19 (MT20570) that contributed to the results presented here.

Conflicts of interest

There are no conflicts to declare.

Notes and references

1 P. Gütlich and H. A. Goodwin (eds), *Spin Crossover in Transition Metal Compounds I–III: Topics in Current Chemistry*, Springer-Verlag: Berlin, 2004, vols. 233–235.

2 M. A. Halcrow (ed), *Spin-crossover materials – properties and applications,* John Wiley & Sons, Chichester, UK, 2013, p. 568.

3 O. Sato, *Nature Chem.*, 2016, **8**, 644; K. S. Kumar and M. Ruben, *Coord. Chem. Rev.*, 2017, **346**, 176.

4 S. Rat, M. Piedrahita-Bello, L. Salmon, G. Molnár, P. Demont and A. Bousseksou, *Adv. Mater.*, 2018, **30**, 1703862; E. Coronado, *Nature Rev. Mater.*, 2020, **5**, 87.

5 A. B. Gaspar and M. Seredyuk, *Coord. Chem. Rev.*, 2014, **268**, 41; A. Enriquez-Cabrera, A. Rapakousiou, M. P. Bello, G. Molnár, L. Salmon and A. Bousseksou, *Coord. Chem. Rev.*, 2020, **419**, 213396.

6 K. Kuroiwa, *Inorganics*, 2017, **5**, 45.

7 R. Akiyoshi, R. Ohtani, L. F. Lindoy and S. Hayami, *Dalton Trans.*, 2021, doi: 10.1039/d1dt00004g

8 See eg S. Hayami, R. Moriyama, A. Shuto, Y. Maeda, K. Ohta and K. Inoue, *Inorg. Chem.*, 2007, **46**, 7692; M. Seredyuk, A. B. Gaspar, V. Ksenofontov, Yu. Galyametdinov, J. Kusz and P. Gütlich, *J. Am. Chem. Soc.*, 2008, **130**, 1431; M. Seredyuk, A. B. Gaspar, V. Ksenofontov, Yu. Galyametdinov, J. Kusz and P. Gütlich, *Adv. Funct. Mater.*, 2008, **18**, 2089; M. Seredyuk, M. C. Muñoz, V. Ksenofontov, P. Gütlich, Yu. Galyametdinov and J. A. Real, *Inorg. Chem.*, 2014, **53**, 8442; N. Abdullah, N. L. M. Noor, A. R. Nordin, M. A. Halcrow, D. R. MacFarlane, M. A. Lazar, J. M. Pringle, D. W. Bruce, B. Donnio and B. Heinrich, *J. Mater. Chem. C*, 2015, **3**, 2491; M. Seredyuk, K. Znovjyak, M. C. Muñoz, Yu. Galyametdinov, I. O. Fritsky and J. A. Real, *RSC Adv.*, 2016, **6**, 39627.

9 T. Fujigaya, D.-L. Jiang and T. Aida, *J. Am. Chem. Soc.*, 2003, **125**, 14690; T. Romero-Morcillo, M. Seredyuk, M. C. Muñoz and J. A. Real, *Angew. Chem. Int. Ed.*, 2015, **54**, 14777; F.-J. Valverde-Muñoz, M. Seredyuk, M. C. Muñoz, G. Molnár, Y. S. Bibik and J. A. Real, *Angew. Chem. Int. Ed.*, 2020, **59**, 18632.

10 S. Hayami, Y. Shigeyoshi, M. Akita, K. Inoue, K. Kato, K. Osaka, M. Takata, R. Kawajiri, T. Mitani and Y. Maeda, *Angew. Chem. Int. Ed.*, 2005, **44**, 4899; S. Hayami, K. Murata, D. Urakami, Y. Kojima, M. Akita and K. Inoue, *Chem. Commun.*, 2008, 6510; S. Hayami, K. Kato, Y. Komatsu, A. Fuyuhiro and M. Ohba, *Dalton Trans.*, 2011, **40**, 2167; A. V. Vologzhanina, A. S. Belov, V. V. Novikov, A. V. Dolganov, G. V. Romanenko, V. I. Ovcharenko, A. A. Korlyukov, M. I. Buzin and Y. Z. Voloshin, *Inorg. Chem.*, 2015, **54**, 5827.

11 T. Delgado, A. Tissot, L. Guénée, A. Hauser, F. J. Valverde-Muñoz, M. Seredyuk, J. A. Real, S. Pillet, E. Bendeif and C. Besnard, *J. Am. Chem. Soc.*, 2018, **140**, 12870; F. J. Valverde-Muñoz, M. Seredyuk, M. Meneses-Sánchez, M. C. Muñoz, C. Bartual-Murgui and J. A. Real, *Chem. Sci.*, 2019, **10**, 3807.

12 S. Schlamp, B. Weber, A. D. Naik and Y. Garcia, *Chem. Commun.*, 2011, **47**, 7152; J. Weihermüller, S. Schlamp, B. Dittrich and B. Weber, *Inorg. Chem.*, 2019, **58**, 1278.

13 D. Rosario-Amorin, P. Dechambenoit, A. Bentaleb, M. Rouzières, C. Mathonière and R. Clérac, *J. Am. Chem. Soc.*, 2018, **140**, 98.

14 W. Zhang, F. Zhao, T. Liu, M. Yuan, Z.-M. Wang and S. Gao, *Inorg. Chem.*, 2007, **46**, 2541.

15 For other recent examples see eg H. L. C. Feltham, C. Johnson, A. B. S. Elliott, K. C. Gordon, M. Albrecht and S. Brooker, *Inorg. Chem.*, 2015, **54**, 2902; Y.-H. Luo, Q.-L. Liu, L.-J. Yang, Y. Sun, J.-W. Wang, C.-Q. You and B.-W. Sun, *J. Mater. Chem. C,* 2016, **4**, 8061; K. S. Kumar, M. Studniarek, B. Heinrich, J. Arabski, G. Schmerber, M. Bowen, S. Boukari, E. Beaurepaire, J. Dreiser and M. Ruben, *Adv. Mater.*, 2018, **30**, 1705416; B. L. Geoghegan, W. Phonsri, P. N. Horton, J. B. Orton, S. J. Coles, K. S. Murray, P. J. Cragg, M. K. Dymond and I. A. Gass, *Dalton Trans.*, 2019, **48**, 17340; A. Kashiro, W. Kohno and T. Ishida, *Inorg. Chem.*, 2020, **59**, 10163.

16 L. J. Kershaw Cook, R. Mohammed, G. Sherborne, T. D. Roberts, S. Alvarez and M. A. Halcrow, *Coord. Chem. Rev.*, 2015, **289–290**, 2.

17 I. Galadzhun, R. Kulmaczewski, O. Cespedes, M. Yamada, N. Yoshinari, T. Konno and M. A. Halcrow, *Inorg. Chem.*, 2018, **57**, 13761.

18 G. Zoppellaro and M. Baumgarten, *Eur. J. Org. Chem.*, 2005, 2888 and 4201 (correction); S. Basak, P. Hui, S. Boodida and R. Chandrasekar, *J. Org. Chem.*, 2012, **77**, 3620.

19 The preliminary structure solutions of the other isomorphous $[Fe(L^2C_n)_2][BF_4]_2$ crystals yield interbilayer spacings of 34.219(7) Å (n = 16) and 36.453(6) Å (n = 18). The interbilayer spacing in this lattice type shows an apparently linear correlation with n.

20 R. Boča, *Coord. Chem. Rev.*, 2004, **248**, 757.

21 See eg S. Barman, N. V. Venkataraman, S. Vasudevan and R. Seshadri, *J. Phys. Chem. B*, 2003, **107**, 1875; H. Li, W. Bu, W. Qi and L. Wu, *J. Phys. Chem. B*, 2005, **109**, 21669; P. N. Nelson and H. A. Ellis, *Dalton Trans.*, 2012, **41**, 2632; G. Gbabode, M. Dohr, C. Niebel, J.-Y. Balandier, C. Ruzié, P. Négrier, D. Mondieig, Y. H. Geerts, R. Resel and M. Sferrazza, *ACS Appl. Mater. Interfaces*, 2014, **6**, 13413.

22 M. Marchivie, P. Guionneau, J.-F. Létard, D. Chasseau and J. A. K. Howard, *J. Phys. Chem. Solids*, 2004, **65**, 17; G. A. Craig, J. S. Costa, S. J. Teat, O. Roubeau, D. S. Yufit, J. A. K. Howard and G. Aromí, *Inorg. Chem.*, 2013, **52**, 7203; K. D. Murnaghan, C. Carbonera, L. Toupet, M. Griffin, M. M. Dîrtu, C. Desplanches, Y. Garcia, E. Collet, J.-F. Létard and G. G. Morgan, *Chem. Eur. J.*, 2014, **20**, 5613; V. Gómez, C. Sáenz de Pipaón, P. Maldonado-Illescas, J. C. Waerenborgh, E. Martin, J. Benet-Buchholz and J. R. Galán-Mascarós, *J. Am. Chem. Soc.*, 2015, **137**, 11924.

23 See *eg* L. J. Kershaw Cook, J. Fisher, L. P. Harding and M. A. Halcrow, *Dalton Trans.*, 2015, **44**, 9417; I. Šalitroš, O. Fuhr and M. Ruben, *Materials*, 2016, **9**, 585; R. Kulmaczewski, E. Trzop, L. J. Kershaw Cook, E. Collet, G. Chastanet and M. A. Halcrow, *Chem. Commun.*, 2017, **53**, 13268; S. Kuramochi, T. Shiga, J. M. Cameron, G. N. Newton and H. Oshio, *Inorganics*, 2017, **5**, 48.

24 V. A. Money, C. Carbonera, J. Elhaïk, M. A. Halcrow, J. A. K. Howard and J.-F. Létard, *Chem. Eur. J.*, 2007, **13**, 5503.

25 See eg G. Ritter, E. König, W. Irler and H. A. Goodwin, *Inorg. Chem.*, 1978, **17**, 224; Y. Garcia, V. Ksenofontov, S. Mentior, M. Dirtu, C. Gieck, A. Bhatthacharjee and P. Gütlich, *Chem. Eur. J.*, 2008, **14**, 3745; J.-F. Létard, S. Asthana, H. J. Shepherd, P. Guionneau, A. E. Goeta, N. Suemura, R. Ishikawa and S. Kaizaki, *Chem. Eur. J.*, 2012, **18**, 5924; N. Paradis, G. Chastanet, F. Varret and J.-F. Létard *Eur. J. Inorg. Chem.* 2013, 968.

26 S. Brooker, *Chem. Soc. Rev.*, 2015, **44**, 2880.

27 See eg M. S. Shongwe, B. A. Al-Rashdi, H. Adams, M. J. Morris, M. Mikuriya and G. R. Hearne, *Inorg. Chem.*, 2007, **46**, 9558; B. Weber, C. Carbonera, C. Desplanches and J.-F. Létard, *Eur. J. Inorg. Chem.*, 2008, 1589; A. Lennartson, A. D. Bond, S. Piligkos and C. J. McKenzie, *Angew. Chem. Int. Ed.*, 2012, **51**, 11049; Y.-Y. Zhu, H.-Q. Li, Z.-Y. Ding, X.-J. Lü, L. Zhao, Y.-S. Meng, T. Liu and S. Gao, *Inorg. Chem. Front.*, 2016, **3**, 1624; R. Díaz-Torres, W. Phonsri, K. S. Murray, L. Liu, M. Ahmed, S. M. Neville, P. Harding and D. J. Harding, *Inorg. Chem.*, 2020, **59**, 13784.

28 M. Shatruk, H. Phan, B. A. Chrisostomo and A. Suleimenova, *Coord. Chem. Rev.*, 2015, **289–290**, 62.

29 L. J. Kershaw Cook, R. Kulmaczewski, R. Mohammed, S. Dudley, S. A. Barrett, M. A. Little, R. J. Deeth and M. A. Halcrow, *Angew. Chem. Int. Ed.*, 2016, **55**, 4327.